2023 9th International Conference on Control, Decision and Information Technologies
CoDIT 2023 | Rome, Italy / July 03-06, 2023 Technically co-sponsored by IEEE & IFAC

Neural Network Control of a SOTM Antenna

Oğuz Kaan Hancıoğlu[1] and Mehmet Önder Efe[2]

2023 9th International Conference on Control, Decision and Information Technologies (CoDIT) | 979-8-3503-1140-2/23/$31.00 ©2023 IEEE | DOI: 10.1109/CODIT58514.2023.10284067

***Abstract*— Satcom on the Move (SOTM) antennas are the primary devices for establishing satellite communication in both military and commercial applications. The main design parameters of the SOTM antennas are low cost, low weight, and high data rate. SOTM antennas are basically two or three degrees of freedom robotic manipulators with an antenna payload. In the classical approach, a position and stabilization controller is implemented in order to achieve a high data rate. Most applications use a tracking algorithm to find the maximum RF signal strength by planning a special trajectory for the end effector. In this article, SOTM antennas are modeled and controlled as if they are robotic manipulators. In addition, a neural network controller is implemented to control the robot manipulator and find the maximum RF signal. The neural network controller includes filtered computed torque control (CTM), robustifying signal, and 2 layers neural network structure. The filtered CTM and robustifying signal ensure the closed-loop characteristic, while the neural network structure eliminates nonlinearities and generates the required torque to find the maximum RF signal. The results obtained through a series of simulations demonstrate the desired qualities.**

I. INTRODUCTION

SATCOM on the Move (SOTM) antennas can find and track the satellite on land, air, and sea platforms. They are the multidisciplinary devices that establish the connection between the platform and the satellite. To overcome military requirements, the development of SOTM antennas began. Thanks to the advances in satellite technologies, SOTM antennas have been used on commercial platforms. Currently, they are used on different platforms in order to compensate for both military and commercial needs.

In fact, the SOTM antenna is a robotic manipulator with an antenna payload. The payload consists of a directional antenna and RF components that are responsible for communication with the satellite [1]. The aperture is where the RF signal is received and transmitted. In the high-speed SOTM application, the SOTM antenna must point to the aperture with maximum gain [2]. The aperture gain depends on the pitch and yaw angle of the end effector. The pointing error is the difference between the actual RF signal and the maximum RF signal. Mobility is one of the key parameters for designing the SOTM antenna. Mobility is directly related to the pointing error. The SOTM antenna must be capable of pointing under various disturbances with low pointing error to communicate at high speed [3], [4].

*This work was supported by Turkish Aerospace Inc.

[1]Oğuz Kaan Hancıoğlu is with the Autopilot Systems, Helicopter Executive Vice Presidency, Turkish Aerospace Inc., 06980, Ankara, Turkey oguzkaan.hancioglu@tai.com.tr

[2]Mehmet Önder Efe is with the Department of Computer Engineering, Hacettepe University, 06800, Ankara, Turkey onderefe@ieee.org

Antenna type and communication frequency determine the pointing accuracy of the robotic manipulator. Pointing accuracy depends on communication frequency and antenna diameter but is limited to 0.2° by the Federal Communications Commission (FCC) [5]. In order to obtain the ALLSAT license, which is an important license in the commercial market, the pointing accuracy must be less than 0.2°. The FCC prohibits transmission when the pointing error is greater than 0.2°. However, there is no limitation in the receiving operation. Unfortunately, higher pointing accuracy in the receiving will result in wider bandwidth leasing from a satellite in order to have the same data speed. This situation will increase the operation cost of SOTM antennas [6].

Two-axis robotic manipulators are a common solution for SOTM antennas due to their low cost. This manipulator is called the Azimuth-Elevation and corresponds to the yaw-pitch manipulator. However, the redundancy occurs, when the elevation angle comes close to 90°. In this case, the azimuth axis cannot contribute to the end effector. This problem can be alleviated by adding an extra axis. The three-axis manipulator is called Azimuth - Canted-level - Elevation and corresponds to the yaw/roll/pitch manipulator [2].

The kinematic model of the SOTM antenna was evaluated by calculating sequential rotation matrices characterized by the separated rotation axis [7]–[9]. This method reduces the complexity of kinematic modeling while making the system more complex to control. SOTM antennas were first studied as a robotic manipulator in [10]. Kinematic modeling using the Denavit-Hartenberg method is a difficult problem, as the SOTM antenna is a special manipulator and is compatible with the GPS coordinate system. This modeling was accomplished by adding an imaginary axis between the azimuth and the canted-level axis. The imaginary axis hinders dynamical modeling and obtaining the Jacobian operator. This problem was resolved by shifting the canted-level axis over the elevation axis [11].

The dynamic model of the SOTM antenna was created using sequential Newtonian dynamics equations in previous studies [7], [8]. The main reason for this approach was to calculate how much torque would be required to stabilize the end effector due to mobile platform motion. In a different study, the SOTM antenna has been modeled and controlled as a single input single output (SISO) system [11]. In the study, complex robot dynamics and the behavior of SISO systems are examined. The difference between them was very small. This is the result of using the mass stabilization technique and radome. Mass stabilization is the name of the mechanical design method that aims to coincide with the rotation axis and the center of inertia. The radome is the mechanical

structure that covers the SOTM antenna from rain, wind, and other external conditions [12]. Thus, the robotic manipulator can be simulated as if it is working in free space.

The mobile platform movement is the main disturbance for the SOTM antenna. SOTM antenna payload should have the correct look angles in order to maintain communication. Due to sensors' accuracy and platform movement, the calculation of look angles is achieved with errors. These errors will cause a pointing error for the SOTM antenna. RF signal should be used to reduce the pointing error. However, the RF signal cannot be used as feedback to the position controller. This is because the RF signal depends on the pitch and yaw angle of the end effector. Therefore, the RF signal feedback is performed by using scanning algorithms. These algorithms are special algorithms for the end effector of a robotic manipulator. Scanning algorithms calculate the trajectories by measuring the RF signal strength. The manipulator's axes references are calculated using the robotic manipulator's inverse kinematic. Step track and conical scan algorithms are widely used in SOTM applications [13], [14].

The neural network based control was initially implemented to the robotic manipulator in [15]. In this approach, the neural network functions as an additional controller to the filtered CTM. The filtered CTM ensures the stability of the robot manipulator, while the neural network eliminates the uncertainties of the system. This approach is a good model-free approach to improve controller performance under unknown uncertainties. Moreover, this neural network structure implemented different robot control problems to solve the nonlinearities [16], [17].

In this article, a three-axis SOTM antenna will be modeled and controlled as a robotic manipulator. In the kinematic modeling, the sliding axis assumption will be used for the three-axis robotic manipulator. This model has not been completed using the GPS coordinate system. This will be solved by adding extra axes to the kinematic model of the antenna. The neural network controller which is described in [15] is implemented as a position controller. RF signal is added into both the neural network structure and the update algorithm to point and maximize RF signal. Therefore, both pointing and maximizing the RF signal are accomplished by the neural network controller.

II. ROBOT KINEMATICS AND DYNAMICS

A. Kinematics

The coordinate systems of the three-axis robotic manipulator are assigned in Fig. 1. The first three axes which are called Azimuth (x_0, y_0, z_0), Canted-level (x_1, y_1, z_1), and Elevation (x_2, y_2, z_2), are responsible for pointing and stabilization. The Polarization (x_3, y_3, z_3) is used to change RF signal polarity and is not required for every SOTM antenna. The polarization axis is added to obtain the full kinematic model. The x_4, y_4, z_4 axis represents the end effector.

In this approach, it is assumed that the canted-level axis coincides with the elevation axis [11]. In this way, we are able to construct a transformation matrix between each sequential axis. To be able to work with the GPS coordinate

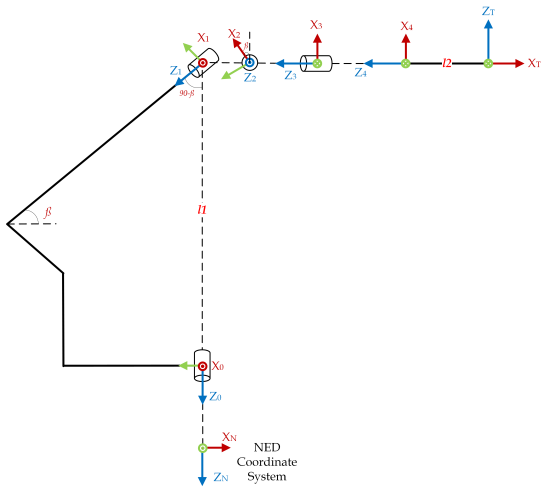

Fig. 1. The axis placement of the three-axis robotic manipulator

system we need to add a base frame before the azimuth axis and an end frame after the end effector axis. The x_n, y_n, z_n must be assigned according to the North-East-Down coordinate system. The x_t, y_t, z_t must correspond to the roll, pitch, and yaw axis, respectively. Since the x_n, y_n, z_n and x_t, y_t, z_t frames are fixed, there is no need to define them in the Denavit-Hartenberg table. The Denavit-Hartenberg table of the three-axis robotic manipulator is given in Table I.

i	α_i	a_i	d_i	θ_i
1	$90-\beta$	0	$-l_1$	θ_1
2	90	0	0	θ_2+90
3	-90	0	0	$-\theta_3+\beta$
4	0	0	$-l_2$	$-\theta_4$

TABLE I

DH TABLE OF THE THERE-AXIS MANIPULATOR

The forward kinematic of the three-axis robotic manipulator is calculated as follows.

$$\mathbf{T}_n^t = \mathbf{T}_n^0 \mathbf{T}_0^1 \mathbf{T}_1^2 \mathbf{T}_2^3 \mathbf{T}_3^4 \mathbf{T}_4^t \tag{1}$$

where the $\mathbf{T}_n^0$ and $\mathbf{T}_4^t$ are given below.

$$\mathbf{T}_n^0 = \begin{bmatrix} 0 & 1 & 0 & 0 \\ -1 & 0 & 0 & 0 \\ 0 & 0 & 1 & 0 \\ 0 & 0 & 0 & 1 \end{bmatrix} \tag{2}$$

$$\mathbf{T}_4^t = \begin{bmatrix} 0 & 0 & 1 & 0 \\ 0 & 1 & 0 & 0 \\ -1 & 0 & 0 & 0 \\ 0 & 0 & 0 & 1 \end{bmatrix} \tag{3}$$

The Azimuth and elevation axes are sufficient for pointing the robot working space [2]. The Canted-level axis works on the stabilization. This situation shows the redundant structure of the robotic manipulator. The inverse kinematic equations of the three-axis robotic manipulator can be mitigated by taking the canted level axis position as zero. Therefore,

(1) can be solved by considering this assumption. The inverse kinematics solution of the azimuth, elevation, and polarization axes can be calculated respectively.

$$\theta_3 = (atan2(a,b) + atan2(-\sqrt{(}a^2+b^2-c^2), c)) + \beta \quad (4)$$

where the $a = 0.866$, $b = 0.5$ and $c = -r_{(3,1)}$.

$$\theta_1 = atan2(\frac{r_{(2,1)}}{d}, \frac{r_{(1,1)}}{d}) \quad (5)$$

where $d = a\cos(\theta_3 - \beta) - b\sin(\theta_3 - \beta)$.

$$\theta_4 = atan2(\frac{r_{(3,2)}}{d}, \frac{r_{(3,3)}}{d}) \quad (6)$$

where $r_{(i,j)}$ is the i^{th} row and j^{th} column element of the desired rotation matrix.

B. Dynamics

In this study, Lagrange-Euler dynamical modeling has been used to develop the dynamical model for the three-axis robotic manipulator. Since SOTM antennas are specialized manipulators, the mechanical design of the manipulator was generally completed using mass stabilization. Therefore, the center of the mass and the axis of rotation are adjacent for each axis. The mechanical parameters (inertia, length, mass of each axis) of the robotic manipulators are taken from [12].

The dynamic equation of the three-axis robotic manipulator is shown in (7).

$$\boldsymbol{\tau} = \mathbf{M}(q)\ddot{\boldsymbol{q}} + \mathbf{V}_m(q,\dot{q})\dot{\boldsymbol{q}} + \mathbf{G}(q) + \mathbf{F}(\dot{q}) + \boldsymbol{\tau_d} \quad (7)$$

where the $\boldsymbol{q} \in \mathbb{R}^3$ is the joint variable vector, $\mathbf{M}(q)$ is the inertia matrix, $\mathbf{V}_m(q,\dot{q})$ is the Coriolis and centripetal matrix, $\mathbf{G}(q)$ is the gravity vector, and $\mathbf{F}(\dot{q})$ is the friction. $\boldsymbol{\tau_d}$ represents bounded unknown disturbance and the torque τ is the control input.

III. ROBOT CONTROL

A. Tracking Error Dynamics

Given a desired joint trajectory $\boldsymbol{q_d} \in \mathbb{R}^3$, the tracking error is represented in (8).

$$\boldsymbol{e} = \boldsymbol{q_d} - \boldsymbol{q} \quad (8)$$

The filtered tracking error in robotics is used and defined as given below.

$$\boldsymbol{r} = \dot{\boldsymbol{e}} + \lambda \boldsymbol{e} \quad (9)$$

where λ is a symmetric positive definite design parameter matrix. the controller guarantees that $\boldsymbol{e}$ is bounded. Therefore the $\boldsymbol{r}$ is bounded. Combining the (7) and derivative of (9), the robot dynamics with respect to filtered tracking error can be written as,

$$\mathbf{M}\dot{\boldsymbol{r}} = -\mathbf{V}_m\boldsymbol{r} - \boldsymbol{\tau} + \boldsymbol{f} + \boldsymbol{\tau_d} \quad (10)$$

where the $\boldsymbol{f}$ is the nonlinear robot function and is given in (11).

$$\boldsymbol{f}(x) = \mathbf{M}(q)(\ddot{\boldsymbol{q_d}} + \lambda\dot{\boldsymbol{e}}) + \mathbf{V}_m(q,\dot{q})(\dot{\boldsymbol{q_d}} + \lambda\boldsymbol{e}) + \mathbf{G}(q) + \mathbf{F}(\dot{q}) \quad (11)$$

where the $\boldsymbol{x} = [\boldsymbol{e}^T, \dot{\boldsymbol{e}}^T, \boldsymbol{q}_d^T, \dot{\boldsymbol{q}}_d^T, \ddot{\boldsymbol{q}}_d^T]$. The computed torque control is commonly used in robotics and calculates the required torque input for given trajectory.

$$\boldsymbol{\tau} = \hat{\boldsymbol{f}} + \mathbf{K}_v\boldsymbol{r} - \boldsymbol{v} - \boldsymbol{v}_{rf} \quad (12)$$

where the $\mathbf{K}_v$ is a controller gain matrix and is usually selected diagonal. $\hat{\boldsymbol{f}}$ is the estimation of the nonlinear robot function. $\mathbf{K}_v\boldsymbol{r} = \mathbf{K}_v\dot{\boldsymbol{e}} + \mathbf{K}_v\lambda\boldsymbol{e}$ is a proportional-derivative (PD) tracking loop, and $\boldsymbol{v}$ is a robustifying signal that provides robustness for unmodelled dynamics and unstructured disturbances. $\boldsymbol{v}_{rf}$ is a robustifying signal for the RF signal and provides the torque needed to point the payload where the signal has the maximum power. Using this control structure, the closed loop system can be represented as,

$$\mathbf{M}\dot{\boldsymbol{r}} = -(\mathbf{K}_v + \boldsymbol{V_m})\boldsymbol{r} + \tilde{\boldsymbol{f}} + \boldsymbol{\tau_d} + \boldsymbol{v} + \boldsymbol{v_{rf}} \quad (13)$$

B. Neural Network Controller for Robot Arms

In this application, the 2 layer feedforward neural network architecture is used. $\mathbf{V}$ and $\mathbf{W}$ are the weights of the 2 layer feedforward neural network. Each output can be calculated using (14). The sigmoid activation function is used in neural network structure.

$$y_i = \sum_{j=1}^{N_h}\left[w_{ij}\sigma\Big(\sum_{k=1}^{n} v_{jk}x_k + \theta_{vj}\Big) + \theta_{wi}\right] \quad (14)$$

The expression in (14) can be written as a matrix form by collecting all v_{jk} and w_{ij} gains into the $\mathbf{V}^T$ and $\mathbf{W}^T$ matrices, respectively. The overall function of the neural network equation is shown in (15).

$$\boldsymbol{y} = \mathbf{W}^T\sigma(\mathbf{V}^T\boldsymbol{x}) \quad (15)$$

Combining (15) and (13), the error dynamics of a neural network control structure can be obtained as,

$$\begin{aligned}\mathbf{M}\dot{\boldsymbol{r}} = &-(\mathbf{K}_v + \mathbf{V}_m)\boldsymbol{r} - \mathbf{W}^T\sigma(\mathbf{V}^T\boldsymbol{x}) - \hat{\mathbf{W}}\sigma(\hat{\mathbf{V}}^T\boldsymbol{x}) \\ &+(\boldsymbol{\epsilon} + \boldsymbol{\tau_d}) + \boldsymbol{v} + \boldsymbol{v}_{rf}\end{aligned} \quad (16)$$

where the $\boldsymbol{\epsilon}$ is the neural network error approximation and $\boldsymbol{\tau_d}$ is the robot disturbances. Both $\boldsymbol{\epsilon}$ and $\boldsymbol{\tau_d}$ excite the error dynamics. The control torque input, neural network weights, robustifying signal, and robustifying RF signal are computed using (17)-(21), respectively.

$$\boldsymbol{\tau} = \hat{\mathbf{W}}^T\sigma(\hat{\mathbf{V}}^T\boldsymbol{x}) + \mathbf{K}_v\boldsymbol{r} - \boldsymbol{v} - \boldsymbol{v_{rf}} \quad (17)$$

$$\begin{aligned}\dot{\hat{\mathbf{W}}} = &\mathbf{F}\sigma(\hat{\mathbf{V}^T}\boldsymbol{x})\boldsymbol{r}^T - \mathbf{F}\hat{\sigma}'\hat{\mathbf{V}}^T\boldsymbol{x}\boldsymbol{r}^T - \kappa\mathbf{F}||\boldsymbol{r}||_2\hat{\mathbf{W}} \\ &-\kappa_{rf}||RF||_2\mathbf{F}||\boldsymbol{r}||_2\hat{\mathbf{W}}\end{aligned} \quad (18)$$

$$\dot{\hat{\mathbf{V}}} = \mathbf{G}x(\hat{\sigma}'^T\hat{\mathbf{W}}\boldsymbol{r})^T - \kappa\mathbf{G}||\boldsymbol{r}||_2\hat{\mathbf{V}} - \kappa_{rf}||RF||_2\mathbf{G}||\boldsymbol{r}||_2\hat{\mathbf{V}} \quad (19)$$

where $\mathbf{F}$, $\mathbf{G}$ positive definite matrices, $\kappa > 0$ and $\kappa_{rf} > 0$.

$$\boldsymbol{v} = -K_z(||\hat{\mathbf{Z}}||_2 + Z_m)\boldsymbol{r} \quad (20)$$

where the $\mathbf{Z} = diag\{\hat{\mathbf{W}}, \hat{\mathbf{V}}\}$, Z_m upper bound on the ideal weight. K_z is the robustifying gain of the controller.

$$\boldsymbol{v_{rf}} = -K_{rf}||\hat{\mathbf{Z}}||_2||RF||_2 \quad (21)$$

where K_{rf} is the robustifying RF gain of the controller and RF is the signal strength. The neural network controller given in (17)-(21) ensures that the system follows the desired trajectory. Details of the proof can be viewed in [18]. The neural network controller guarantees that the tracking error ($\boldsymbol{r}$) and neural network gains ($\hat{\mathbf{W}}$ and $\hat{\mathbf{V}}$). To achieve a small tracking error, a large $\mathbf{K}_v$ gain is required, [15].

The structure of the neural network control of the robot manipulator is shown in Fig. 2, where the $\boldsymbol{q_{ref}}$ is the reference joint angles and $\boldsymbol{q_N}$ is the base disturbance. Inverse kinematics calculates desired trajectories $\boldsymbol{q_d}$ for the neural network controller. The $\boldsymbol{e} = [\boldsymbol{e}^T, \dot{\boldsymbol{e}}^T]^T$ and $\boldsymbol{q} = [\boldsymbol{q}^T, \dot{\boldsymbol{q}}^T]^T$. The $\mathbf{K}_v\boldsymbol{r} = \mathbf{K}_v(\dot{\boldsymbol{e}} + \lambda \boldsymbol{e})$ is the PD control and guarantees the stability of the filtered tracking error $\boldsymbol{r}$ with robustifying signal $\boldsymbol{v}$. The input of the neural network can be taken as (22).

$$\boldsymbol{x} = [\boldsymbol{\zeta_1}^T, \boldsymbol{\zeta_2}^T, \cos(\boldsymbol{q})^T, \sin(\boldsymbol{q})^T, \dot{\boldsymbol{q}}, \text{sign}(\dot{\boldsymbol{q}}), RF, eRF] \quad (22)$$

where the $\boldsymbol{\zeta_1} = \ddot{\boldsymbol{q}}_{\boldsymbol{d}} + \lambda \dot{\boldsymbol{e}}$, $\boldsymbol{\zeta_2} = \dot{\boldsymbol{q}}_{\boldsymbol{d}} + \lambda \boldsymbol{e}$, RF is the beacon receiver signal output, eRF is the difference between maximum RF signal strength and output.

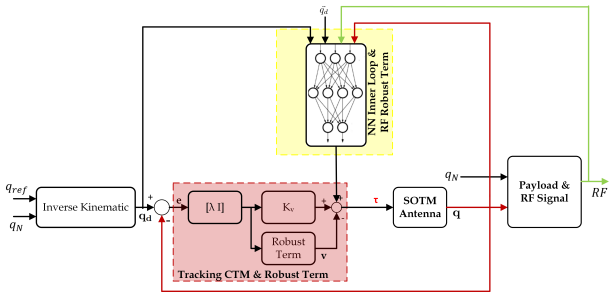

Fig. 2. Neural network controller for the SOTM antenna

IV. RESULTS

A beacon receiver is a device that measures the RF signal strength. It produces 10 V for the maximum signal and 0 V for the minimum signal. Maximum and minimum values can be set to beacon receivers using serial communication. In this article, a 1 m reflector antenna and Ku band communication system are modeled and used. The antenna's maximum signal is modeled as 10 V and the minimum signal is modeled as 0 V. The detail of the antenna system can be found in [12].

The neural network controller finds the maximum RF signal value by producing $\boldsymbol{v_{rf}}$ signal. This signal must be directional to find the maximum signal strength. However, the neural network cannot determine the direction of each axis. The step track algorithm determines the axis direction for $\boldsymbol{v_{rf}}$ signal. Before the neural network controller, the step track algorithm finds the direction of each axis. Then the signal $\boldsymbol{v_{rf}}$ applies the required torque using direction.

The controller parameters are taken the $\mathbf{K}_v = diag\{20,20\}$ and $\lambda = diag\{5,5\}$. The weight tuning design parameters are taken as $\mathbf{F} = diag\{10,10\}$, $\mathbf{G} = diag\{10,10\}$, $N_h = 15$, $\kappa = 0.1$, and $\kappa_{rf} = 0.5$. The parameters K_z and K_m are taken 50 for robustifying signal. The K_{rf} is taken 1200 for the robustifying RF signal. The base disturbance in the simulation is taken as $\boldsymbol{q_N} = [6sin(0.63t), 5sin(0.75t), 3sin(0.63t]^T$.

Modeling the causes of pointing errors in simulations is a difficult issue. Therefore, the performance of the neural network controller can be tested starting from four different starting points. the pointing error in each starting point is bigger than 0.2°. The maximum signal strength is set to $\boldsymbol{q} = [160.6, 0, 40.7]^T$. It is expected from the simulations, the neural network controller will reach the maximum signal by minimizing the pointing error with/without base disturbance. In Fig. 3 and 5, each line represents an equivalent azimuth-elevation angle from the different starting points, without and with base disturbance respectively. In Fig. 4 and 6, each line represents the pointing error of the different starting points without and with base disturbance, respectively. The neural network controller tries to find the maximum signal strength in each simulation.

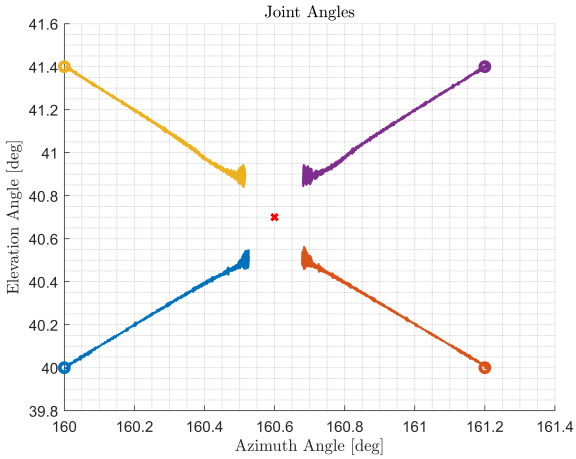

Fig. 3. Equivalent azimuth elevation angles without base disturbance

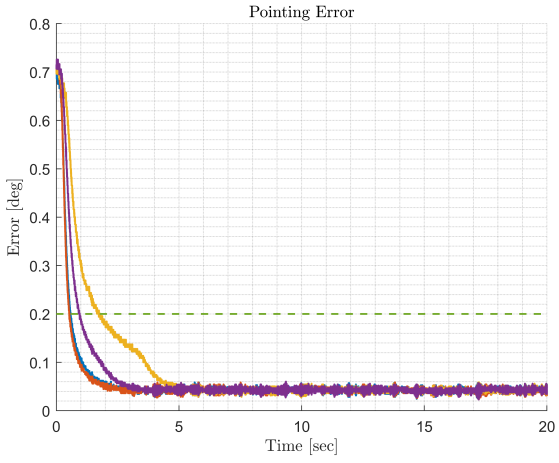

Fig. 4. Pointing error of the SOTM antenna without base disturbance

Fig. 5 demonstrates the equivalent azimuth-elevation angle. The azimuth and elevation angles are constantly chang-

ing due to the disturbance. In order to illustrate these changes, forward kinematics $\mathbf{T}_n^t$ is solved without considering the disturbance. Thus, the equivalent azimuth elevation angles are obtained. The neural network controller almost reaches almost the maximum signal point in both conditions as shown in Fig. 4 and 6. The pointing error drops below 0.2° in 4 seconds without base disturbance and below 0.2° in about 1.5 seconds with base disturbance. In both conditions pointing error reaches 0.05°.

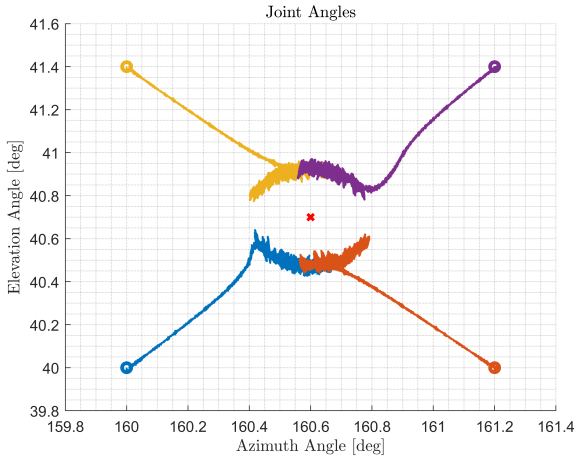

Fig. 5. Equivalent azimuth elevation angles with base disturbance

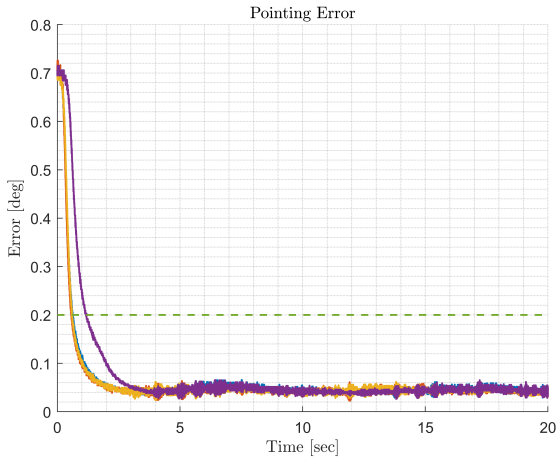

Fig. 6. Pointing error of the SOTM antenna with base disturbance

V. CONCLUSIONS

In the classical approach, the scanning algorithm and position controller establish satellite communication with the maximum RF signal. The scanning algorithm and the position controller are designed and implemented individually. In this study, a multilayer neural network controller was developed for a SOTM antenna. The neural network controller both points and maximizes RF signal. The neural network controller ensures that it points where the RF signal is at its maximum, under the condition of receiving the RF signal. The robustifying RF signal requires the direction of each axis. This axis direction is determined by the step track algorithm. Its purpose is to find the axis direction which increases the RF signal strength and is only applied for a short time. It is recommended that the reference joint angle change to the maximum signal angle after the maximum signal is reached. The robustifying RF signal produces torque value to find the maximum signal strength. This causes a minor error in the filtered tracking controller. If the reference angle changes, the filtered tracking error will be equal to the very small.

REFERENCES

[1] S. Borisov and A. Shishlov, "Antennas for Satcom-on-the-Move, Review," *2014 International Conference on Engineering and Telecommunication*, Moscow, Russia, 2014, pp. 3-7.

[2] J. Debruin, "Control systems for mobile Satcom antennas," in *IEEE Control Systems Magazine*, vol. 28, no. 1, pp. 86-101, Feb. 2008.

[3] H. Beljour et al., "Army SATCOM on the move technology initiatives," *MILCOM 2009 - 2009 IEEE Military Communications Conference*, Boston, MA, USA, 2009, pp. 1-7.

[4] C. Ozbay, W. Teter, D. He, M. J. Sherman, G. L. Schneider and J. A. Benjamin, "Design and Implementation Challenges in Ka/Ku Dual-Band SATCOM-On-The-Move Terminals for Military Applications," *MILCOM 2006 - 2006 IEEE Military Communications conference*, Washington, DC, USA, 2006, pp. 1-7.

[5] R. Murthy, "On-satellite testing of mobile communication antennas for compliance to VMES, ESV, and other pointing accuracy requirements," *2011 - MILCOM 2011 Military Communications Conference*, Baltimore, MD, USA, 2011, pp. 1812-1817.

[6] R. Murthy, "Performance criteria affecting pointing error and the impact on total cost of ownership," *MILCOM 2012 - 2012 IEEE Military Communications Conference*, Orlando, FL, USA, 2012, pp. 1-6.

[7] F. N. Barnes, "Stable Member Equations of Motion for a Three-Axis Gyro Stabilized Platform," *in IEEE Transactions on Aerospace and Electronic Systems*, vol. AES-7, no. 5, pp. 830-842, Sept. 1971.

[8] B. Ekstrand, "Equations of motion for a two-axes gimbal system," *in IEEE Transactions on Aerospace and Electronic Systems*, vol. 37, no. 3, pp. 1083-1091, July 2001.

[9] J. Zhao, F. Gao, Q. Wu, S. Jin, Y. Wu and W. Jia, "Beam Tracking for UAV Mounted SatCom on-the-Move With Massive Antenna Array," *in IEEE Journal on Selected Areas in Communications*, vol. 36, no. 2, pp. 363-375, Feb. 2018.

[10] O. K. Hancioglu, M. Celik and U. Tumerdem, "Kinematics and Tracking Control of a Four Axis Antenna for Satcom on the Move," *2018 International Power Electronics Conference (IPEC-Niigata 2018 -ECCE Asia)*, Niigata, Japan, 2018, pp. 1680-1686.

[11] J. Najman, M. Bastl, M. Appel, and R. Grepl, "Computationally Fast Dynamical Model of a SATCOM Antenna Suitable for Extensive Optimization Tasks", *AiMT*, vol. 14, no. 1, pp. 21–30, January 2019.

[12] O. K. Hancioglu, " Closed-loop control of the satcom on the move antenna using jacobian operator," M.S. thesis, Mechatronics Engineering Department, Istanbul Technical University., Istanbul, 2019.

[13] M. Richharia, "Design considerations for an earth station step-track system," *Space Communication Broadcasting*, vol. 4, pp. 215-228, August 1986.

[14] Gawronski, W., and Craparo, E. M., "Three scanning techniques for deep space network antennas to estimate spacecraft position", Proc. Interplanet. Netw. Progr. Report, 1-17, 2001.

[15] F. L. Lewis, "Neural network control of robot manipulators," *in IEEE Expert*, vol. 11, no. 3, pp. 64-75, June 1996.

[16] C. Kwan, F. L. Lewis and D. M. Dawson, "Robust neural-network control of rigid-link electrically driven robots," *in IEEE Transactions on Neural Networks*, vol. 9, no. 4, pp. 581-588, July 1998.

[17] K. Guo, Y. Pan and H. Yu, "Composite Learning Robot Control With Friction Compensation: A Neural Network-Based Approach," *in IEEE Transactions on Industrial Electronics*, vol. 66, no. 10, pp. 7841-7851, Oct. 2019.

[18] F. L. Lewis, A. Yesildirek and Kai Liu, "Multilayer neural-net robot controller with guaranteed tracking performance," *in IEEE Transactions on Neural Networks*, vol. 7, no. 2, pp. 388-399, March 1996.